nature COMMUNICATIONS

ARTICLE

Received 1 Oct 2015 | Accepted 24 Feb 2016 | Published 4 Apr 2016

DOI: 10.1038/ncomms11144 OPEN

Microelectrode characterization of coral daytime interior pH and carbonate chemistry

Wei-Jun Cai[1,2], Yuening Ma[1,2], Brian M. Hopkinson[2], Andréa G. Grottoli[3], Mark E. Warner[1], Qian Ding[2,4], Xinping Hu[2,5], Xiangchen Yuan[2,6], Verena Schoepf[3,7], Hui Xu[2,4,8], Chenhua Han[2,4,9], Todd F. Melman[10], Kenneth D. Hoadley[1], D. Tye Pettay[1], Yohei Matsui[3], Justin H. Baumann[3], Stephen Levas[3], Ye Ying[4] & Yongchen Wang[2,‡]

Reliably predicting how coral calcification may respond to ocean acidification and warming depends on our understanding of coral calcification mechanisms. However, the concentration and speciation of dissolved inorganic carbon (DIC) inside corals remain unclear, as only pH has been measured while a necessary second parameter to constrain carbonate chemistry has been missing. Here we report the first carbonate ion concentration ($[CO_3^{2-}]$) measurements together with pH inside corals during the light period. We observe sharp increases in $[CO_3^{2-}]$ and pH from the gastric cavity to the calcifying fluid, confirming the existence of a proton (H^+) pumping mechanism. We also show that corals can achieve a high aragonite saturation state (Ω_{arag}) in the calcifying fluid by elevating pH while at the same time keeping [DIC] low. Such a mechanism may require less H^+-pumping and energy for upregulating pH compared with the high [DIC] scenario and thus may allow corals to be more resistant to climate change related stressors.

[1] School of Marine Science and Policy, University of Delaware, Newark, Delaware 19716, USA. [2] Department of Marine Sciences, University of Georgia, Athens, Georgia 30602, USA. [3] School of Earth Sciences, The Ohio State University, Columbus, Ohio 43210, USA. [4] Ocean College, Zhejiang University, Hangzhou 310058, China. [5] Department of Physical and Environmental Sciences, Texas A&M University – Corpus Christi, Corpus Christi, Texas 78412, USA. [6] Key Laboratory of Marine Bio-resources Sustainable Utilization, South China Sea Institute of Oceanology, Chinese Academy of Sciences, Guangzhou 510301, China. [7] ARC Centre of Excellence for Coral Reef Studies, School of Earth and Environment and UWA Oceans Institute, University of Western Australia, Crawley, Western Australia 6009, Australia. [8] School of Mechanical Engineering and Automation, Zhejiang Sci-Tech University, Hangzhou 310023, China. [9] Key Laboratory of Marine Ecosystem and Environment, State Oceanic Administration (SOA) Second Institute of Oceanography, Hangzhou 310012, China. [10] Reef Systems Coral Farm, New Albany, Ohio 43054, USA. Correspondence and requests for materials should be addressed to W.-J.C. (email: wcai@udel.edu).

‡Deceased

Atmospheric CO_2 has increased from 280 parts per million (ppm) during pre-industrial times to 400 ppm today[1]. This increase has led to invasion of CO_2 into the surface ocean, which has shifted the acid–base equilibrium and modified the dissolved inorganic carbon (DIC) species composition such that the proton concentration ($[H^+]$) has increased, and pH and $[CO_3^{2-}]$ have decreased; a process commonly known as ocean acidification (OA)[2,3]. Since OA reduces calcification rates in many, though not all, corals[4–8], it is particularly detrimental to the health of coral reefs and their associated ecosystem functions and biogeochemical processes[4,7,9]. The decline in coral calcification rates is thought to be linked to reductions in seawater $[CO_3^{2-}]$ and thus Ω_{arag}. However, because calcification occurs in a semi-isolated compartment where conditions are largely controlled by the coral[10], the exact mechanism by which OA reduces calcification is difficult to decipher[11]. To understand and predict how corals might respond to current and future CO_2 increases, climate warming and other stressors, we need a better understanding of coral calcification mechanisms, particularly how a high pH and Ω_{arag} state is achieved inside the calcifying fluid and the sources as well as speciation and concentration of DIC that sustain calcification[5,11–16].

In order to precipitate $CaCO_3$ in a place separated from seawater by multiple layers of tissue, corals ultimately must be able to import Ca^{2+} ions and DIC from seawater and transport them to the site of calcification. These processes remain poorly understood and controversial. Although proposed routes of ion and molecule import differ in their details, potential import processes can be broadly grouped into three categories: (1) passive CO_2 diffusion, (2) active bicarbonate and other ion transport and (3) whole seawater import though the time scale of each of these processes will differ[10,16–19]. Which of these three processes dominates the import pathway for DIC species remains unknown in part because a complete characterization of the internal carbonate chemistry of corals is lacking. In addition to the import of necessary ions, corals must raise the aragonite saturation state of the calcifying fluid to obtain rapid rates of calcification[18]. It is widely believed that this is achieved through a H^+ efflux pump that creates high pH and, via chemical equilibrium and kinetic limitations, high $[CO_3^{2-}]$ in the calcifying space[5,19]. The H^+ efflux pump is proposed to be coupled to Ca^{2+} influx via a Ca–H ATPase[10]. This theoretical model for coral calcification is considered the foundation for hypotheses explaining the response of calcification to future acidification[5], yet direct measurements of at least two of the several carbonate system parameters to fully substantiate this conceptual model for coral calcification are lacking. Based on either indirect geochemical tracer evidence[12] or sensor-based pH data combined with the assumption of either active HCO_3^- transport or whole seawater import[13,20], several studies have also suggested that corals concentrate DIC to roughly twice the seawater value at the site of calcification. Others, however, have assumed that coral internal [DIC] is similar to or lower than that in seawater[5,21]. Furthermore, while a linkage between H^+-pumping and carbon species transportation has recently been suggested[12], confirmation by direct measurements is required. In summary, despite decades of research, our knowledge of the internal carbonate chemistry of corals is still limited and direct evidence is needed to definitively constrain coral calcification mechanisms.

Microelectrodes are a powerful tool for the direct measurement of chemical concentrations within organisms. The reliability and accuracy of pH and other microelectrodes have been well-established in the literature and in our work (see Methods section below). Previous pH microelectrode studies have shown that pH increases near the coral surface and in the upper region of the polyp's gastric cavity due to photosynthesis, but decreases deeper in the cavity (coelenteron)[22]. Most importantly, a high pH has been measured in the calcifying fluid using both pH microelectrodes (pH: 9.3–10.1) and pH sensitive dyes (pH: 8.5–9.0) (refs 5,13,23). These experiments showed that corals increase the pH of the calcifying fluid to achieve a high Ω_{arag}, which facilitates rapid rates of calcification. However, to fully characterize internal coral carbonate chemistry, pH alone is not sufficient and another carbonate system parameter such as $[CO_3^{2-}]$, [DIC], or total alkalinity (TA) must be assumed[12,13] or preferably directly measured.

Here we use CO_3^{2-} microelectrodes together with pH microelectrodes to directly measure two necessary system parameters and calculate concentrations of all other carbonate species within corals. Our novel findings are that $[CO_3^{2-}]$ and carbonate saturation state inside the coral calcifying fluid are high and calcifying fluid DIC concentration is low.

Results

pH and $[CO_3^{2-}]$ depth profiles. pH and CO_3^{2-} microelectrodes were used to characterize the interior of coral polyps (see Methods section below) under ambient seawater pH and in the light (500 µmol photons $m^{-2} s^{-1}$), when photosynthesis stimulates high rates of calcification. We advanced a microelectrode inside the polyp's gastric cavity at a resolution of 50 µm per step (5 µm in one case) parallel to the polyp wall until it broke on the solid $CaCO_3$ base (Fig. 1a,b). Repeated micro-profile measurements from seawater into the lower part of the coelenteron revealed that the profiles were reproducible (Fig. 1b, Supplementary Figs 1a,b and 2) even though polyp contraction sometimes affected the observed depths (Supplementary Fig. 2) and introduced noise in the electrode data.

We obtained several full-depth profiles of pH and CO_3^{2-} through the polyp mouth, the coelenteron, and into the calcifying fluid for three tropical coral species: *Orbicella faveolata, Turbinaria reniformis* and *Acropora millepora*. For *O. faveolata*, pH (in National Bureau of Standards, NBS, scale) increased from 8.1 and $[CO_3^{2-}]$ from 180 µmol kg^{-1} in the overlying seawater to 8.3–8.5 and ~300 µmol kg^{-1}, respectively, in the upper part of the polyp due to photosynthesis (Fig. 2a,b). Deeper in the polyps the pH decreased to a value of 7.7, which was consistent with earlier studies[13,22,24]. Correspondingly, in the deeper portion of the polyp, $[CO_3^{2-}]$ decreased to 100 µmol kg^{-1}. Then, within a short distance, pH increased sharply to as high as 9.7, confirming previous work[5,13,23], while $[CO_3^{2-}]$ increased six fold to 600 µmol kg^{-1} before the electrode tip broke. We interpret this rapid increase in pH and $[CO_3^{2-}]$ as evidence that the microelectrodes obtained measurements within the calcifying fluid prior to breaking.

Similar profiles were measured inside coral polyps of *T. reniformis* with highest pH in the calcifying fluid ranging from 8.8 to 9.3 (Fig. 2c) and highest $[CO_3^{2-}]$ from 1000 to 1400 µmol kg^{-1} (Fig. 2d). In *A. millepora*, the electrode advancement step was reduced to 5 µm due to the smaller polyps compared with the other species, resulting in a very fine-scale pH profile, which demonstrated a sharp increase in pH from 8.15 to 8.65 within only a short distance of 10–60 µm (Fig. 2c). Similarly, we observed a 15-fold increase in $[CO_3^{2-}]$ from ~100 µmol kg^{-1} in the coelenteron to ~1500 µmol kg^{-1} in the calcifying fluid within a distance of 50 µm in this species (Fig. 2d).

Composite depth profiles of CO_2, DIC, TA and Ω_{arag}. Our methods did not allow simultaneous profiling of pH and $[CO_3^{2-}]$ at the same spots due to both technical challenges and high heterogeneity inside a coral polyp. Therefore, we constructed composite profiles of pH and $[CO_3^{2-}]$ based on the range of

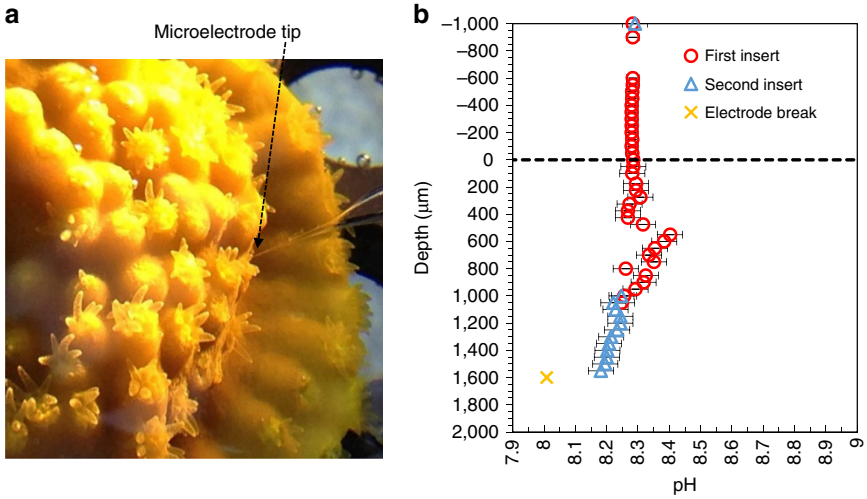

Figure 1 | Microelectrode profiling and electrode performance. (**a**) Close-up view of the coral *T. reniformis* showing the tip of a microelectrode as it enters the polyp. (**b**) Repeated pH microelectrode profile readings inside a *T. reniformis* coral polyp. Between the last point of the second insert and the next reading (which is a noise-free reading and is marked as ×), the microelectrode tip broke. pH microelectrodes were calibrated on the NBS scale, which is about 0.1–0.15 unit greater than that on the total scale. Error bars (s.d.) are defined in the Methods section. Positive depths are inside the coral polyp while negative depths are in the overlying seawater. Error bars are smaller than the symbols in the overlying water.

our data across all three species and calculated [CO_2], DIC, TA and Ω_{arag} profiles (Supplementary Table 1), assuming the DIC system was in chemical equilibrium (see Methods section below). These composite profiles were then used to generate a more complete picture and a conceptual model of coral calcification.

Overall, our study shows that DIC decreases slightly near the polyp surface and in the upper part of the coelenteron due to photosynthetic CO_2 consumption (Fig. 3a,b). Farther down in the polyp calculated DIC increases due to respiratory input of CO_2 and reaches a peak at the bottom of the coelenteron before rapidly declining again in the calcifying space (Fig. 3b). Calculated TA in the coelenteron is nearly constant throughout most of the gastric cavity space, but increases dramatically in the calcifying fluid (Fig. 3b). Nonetheless, in agreement with direct TA measurements of the coelenteron fluid[25] and some model assumptions[5,21], DIC and TA values in the coelenteron solution are not substantially different from those of the overlying seawater.

Notably, a sharp increase in [CO_2] to $\sim 30\,\mu mol\,kg^{-1}$ occurs toward the bottom of the coelenteron solution (Fig. 3b). This increase is not only due to an increase in DIC from respiration but is substantially enhanced by the nearly invariable TA (Fig. 3b, Supplementary Table 1). Thus, we attribute this [CO_2] increase to both respiration input and the conversion of CO_3^{2-} and HCO_3^- to CO_2 by H^+ exported from the calcifying fluid (Fig. 3a) – a mechanism suggested earlier as being important for *Symbiodinium* spp. photosynthetic needs[19]. Inside the calcifying fluid [CO_2] is nearly zero (Fig. 3b), primarily due to the fluid's very high pH (Fig. 2a,c). This very large [CO_2] difference ($\sim 30\,\mu mol\,kg^{-1}$, Supplementary Table 1), based on direct measurements for the first time, confirms recent indirect evidence from geochemical tracers[12] that a high rate of CO_2 molecular diffusion from the coelenteron through the tissue into the calcifying fluid provides an important source of DIC for $CaCO_3$ precipitation.

CO_2 flux into the calcifying fluid. We estimated the CO_2 influx to the calcifying fluid by both a 1-D diffusion model and an exchange model between the coelenteron and the calcifying fluid[21,26] (equations and parameters are given in the Methods section and Supplementary Table 1). The CO_2 diffusive flux was estimated to be as high as 217–433 $nmol\,cm^{-2}\,h^{-1}$. Alternatively, the CO_2 influx was estimated by the exchange model to be 82–301 $nmol\,cm^{-2}\,h^{-1}$ (see Methods section). This range of CO_2 influx and consumption rate compares favourably with coral calcification rates measured in the past (150–1000 $nmol\,cm^{-2}\,h^{-1}$) (refs 10,27). Based on the observations and model calculations presented here, we postulate that the coral's proton pumping ability is essential not only for creating a high aragonite saturation state in the calcifying fluid (favouring calcification), but also for creating a sharp CO_2 gradient facilitating DIC influx to support calcification. This CO_2 transport mechanism is consistent with dual isotopic evidence[18,28] and geochemical proxies[12] showing that respired CO_2 is an essential source of DIC for calcification. This passive CO_2 transport mechanism may reduce the need for the active transport of HCO_3^- by processes such as transmembrane or vacuolar transport though the ultimate source of DIC for calcification comes from external seawater via photosynthesis, diffusive flux and whole seawater import.

Low [DIC] in the calcifying fluid. Despite the great CO_2 flux into the coral calcifying fluid, our analysis reveals that the fluid [DIC] is not that different from seawater concentrations due to the consumption of DIC during calcification, which balances the CO_2 influx (Fig. 3a). Even though TA in the calcifying fluid is elevated (1.2–1.9 times that of overlying seawater) it is not as high as previously reported values[12]. Allison *et al.*[12] have recently used geochemical tracers to determine pH (from B isotope ratio) and estimate DIC (from B/Ca ratio) and concluded that in order to achieve a high aragonite saturation state, corals must internally concentrate DIC. Others also assumed that corals concentrate internal DIC to about twice, or more, the concentration of seawater[13,29]. Our direct pH and [CO_3^{2-}] measurements show that while Ω_{arag} inside the calcifying fluid is elevated, DIC is not elevated with respect to background seawater.

Discussion

Our microelectrode profiles of pH and CO_3^{2-} through coral polyps provide the first direct evidence for elevated [CO_3^{2-}] in the calcifying fluid. [CO_3^{2-}] (600–1500 $\mu mol\,kg^{-1}$) and corresponding aragonite mineral saturation states ($\Omega_{arag} = 8–22$) in the calcifying fluid are high and consistent with expectations based on inorganic $CaCO_3$ formation experiments[11], previous experiments[12] and model frameworks[5,13].

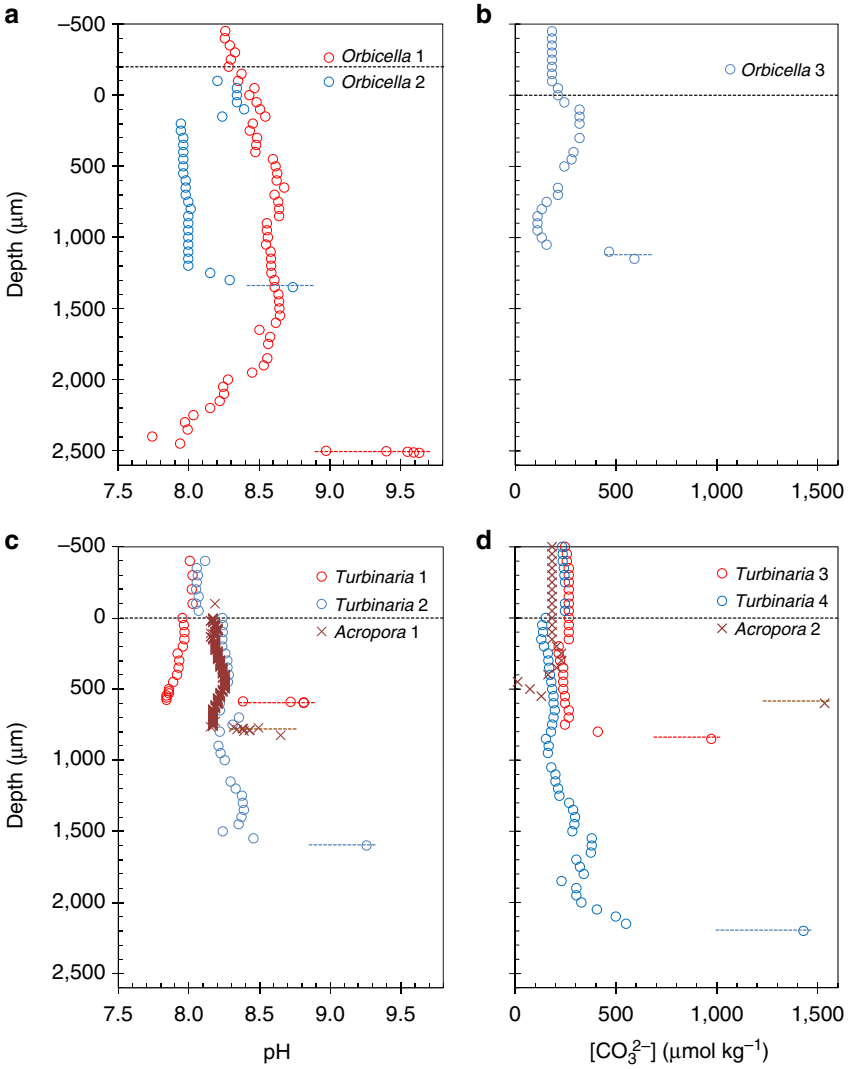

Figure 2 | Coral internal pH and [CO_3^{2-}] profiles through the polyp mouths. (**a**) pH and (**b**) [CO_3^{2-}] of *Orbicella faveolata* corals. (**c**) pH and (**d**) [CO_3^{2-}] of *Turbinaria reniformis* and *Acropora millepora* corals. Dashed black lines indicate the top of the polyp mouths. Colored dashed lines roughly indicate the location of the calcifying fluid and differ in depth for each polyp.

Data from the calcifying fluid was only obtained in a small subset of the numerous profiles collected, most likely because the calcifying fluid layer is very thin (likely only a few micrometers) and existed in pockets[13,16,17]. In most cases, the electrode tips broke within one step (50 µm) between the bottom of the polyp gastric cavity space (coelenteron) and the hard $CaCO_3$ skeleton. In some cases, however, the data suggest the space between the coelenteron and the skeleton could be thicker than previously thought (up to 100 µm). Alternatively, it is possible that the newly formed $CaCO_3$ minerals are porous allowing the glass microelectrode tip to slightly penetrate the mineral surface, thus giving an inaccurate measure of the calcifying fluid thickness. It would be desirable to collect profiles with a better constraint of vertical and lateral heterogeneity of carbonate properties inside corals. Nonetheless a high pH, high [CO_3^{2-}] layer was unequivocally detected right above the $CaCO_3$ skeleton, though further work is needed to better define its thickness and assess its spatial variability. While the pH upregulation in the calcifying fluid measured by microelectrodes does overlap with those by the dye-based method[13] and boron isotope method[12], the highest values have been obtained from microelectrodes (9.7 here, 9.3 and 10.1 by two others, see Table 1)[5,23]. Differences between the approaches may result from differences in coral species, colony size[30], measurement condition and location within the colony[13,14], and time-scales over which the approaches integrate[30].

If the very high pH of 9.0 or higher measured by microelectrodes reported here or elsewhere is typical of coral calcifying fluid, a high DIC internal solution (2 × of seawater DIC or higher) would indicate that internal Ω_{arag} could be as high as 30 to 55 (Fig. 4a), which is inconsistent with Ω_{arag} values inferred from abiotic experiments[18]. Therefore, it seems that the most reasonable internal [DIC] is about 1 × of seawater value, which is consistent with our results from the two direct carbonate parameter measurements. While further research is required to confirm our conclusion, our findings strongly shift the argument towards one of a lower calcifying fluid DIC concentration[5,21].

One important difference between low versus high DIC scenarios is the necessary amount of protons that a coral must pump out (which results in an increase in TA) to raise its internal pH by one unit (in mmol-H^+ per kg per pH unit). This buffer index for the high DIC scenario is at least twice that for the low DIC scenario, thus more protons must be removed in a high DIC scenario to achieve the observed calcifying fluid pH (Fig. 4b).

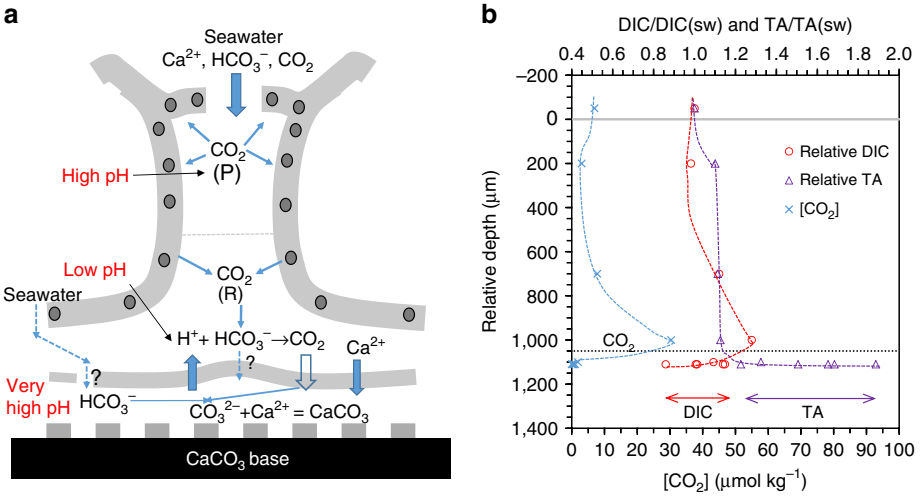

Figure 3 | Conceptual model of coral calcification and CO_2 transport mechanism and distributions of internal [CO_2] and relative DIC and TA to seawater values. (**a**) Illustrative model and (**b**) concentration distributions. Dark circles are photosynthetic endosymbionts. P stands for photosynthesis, R for respiration, and sw for seawater. In (**b**), for DIC (red line) and TA (purple line) the calculated ranges of possible concentrations inside the calcifying fluid are provided based on calculations of all species from Supplementary Table 1.

Table 1 | Comparison of pH values measured in coral calcifying fluid by microelectrodes and other methods.

Technique	Reported by	Coral species	Light condition	Location	pH_T	pH_{NBS}	Notes
Microelectrode	Al-Horani *et al.*[23]	*Galaxea fascicularis* (tropical coral)	Light	Apexes		9.28	Sensor buried under tissue
Microelectrode	Ries[5]	*Astrangia poculata* (temperate coral)	Light	Apexes, between septal ridges		10.1	Through a predrilled incision
Microelectrode	This work	*Orbicella faveolata* (tropical coral)	Light	Apexes, under polyp mouth		8.75–9.65	Sensor penetrated via the mouth
Microelectrode	This work	*Turbinaria reniformis* (tropical coral)	Light	Apexes, under polyp mouth		8.8–9.3	Sensor penetrated via the mouth
Microelectrode	This work	*Acropora millepora* (tropical coral)	Light	Apexes, under polyp mouth		8.65	Sensor penetrated via the mouth
pH sensitive dye	Venn *et al.*[13]	*Stylophora pistillata* (tropical coral; microcolonies)	Light	Distal margin (edge)	8.55–8.85	8.70–9.00	Laterally grown on slide
B-isotopes	Allison *et al.*[12]	*Porites* spp. (tropical coral)	Light/dark cycle	Average	~8.5	~8.65	See citations therein

Note that only one B-isotope based result is given for comparison but many more are cited in the reference. Note, we convert pH_T to pH_{NBS} by adding 0.15.

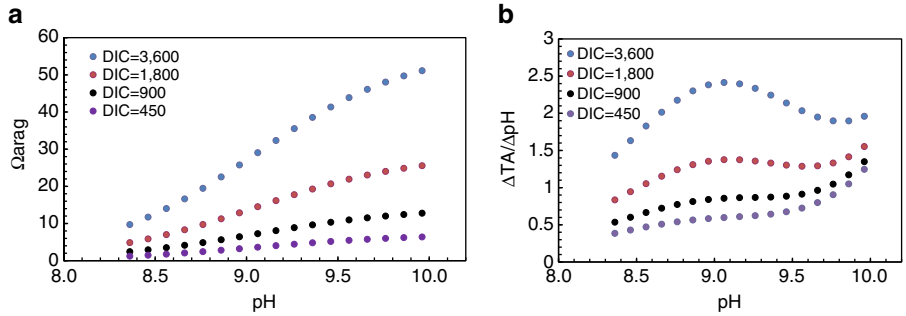

Figure 4 | Aragonite mineral saturation state (Ω_{arag}) and buffer index in the coral calcifying fluid as functions of pH and [DIC]. (**a**) Ω_{arag} and (**b**) buffer index. The buffer index is given as mmol kg^{-1} of H^+ pumping (H^+ loss or TA gain) per unit of pH upregulation. This index is calculated numerically with CO2SYS (ref. 37) (see Methods section). Here [DIC] = 1800 µmol kg^{-1} is roughly the same as seawater value. pH is on the NBS scale.

Therefore, we conclude that the low DIC scenario would require less energy than the high DIC scenario as proton-pumping requires ATP. Comparisons of a relative change in energy requirement to upregulate internal pH between high external CO_2 under future OA conditions and 400 ppm current conditions following the method of Ries[5] also supported our conclusion (Supplementary Note 1 and Supplementary Table 5). As a result, if proton removal from the coelenteron is increasingly

difficult as a result of higher seawater H^+ concentrations under OA conditions[31], the low DIC scenario should be advantageous as less H^+-pumping will be required to further raise pH in the calcifying fluid.

Overall, this suggests that corals that use passive CO_2 diffusion as an important pathway for DIC supply, and maintain low DIC in their calcifying fluid, may require less energy to calcify at high rates, which could potentially make them more resistant to OA and other stressors. However, at the same time, the lower buffering capacity of low DIC and moderate TA calcifying fluid means that the ability to maintain high fluid pH will be vulnerable to changes in the physiological and biochemical conditions that control H^+-pumping. For example, a weakening of proton pumping during dark periods may lead a coral with low internal DIC towards decalcification more readily than otherwise expected in a high DIC scenario. In addition, a high internal DIC could allow corals to reach a high carbonate saturation state at lower internal pH (Fig. 4a)[13]. Therefore, additional studies using microelectrodes and other techniques in corals under OA conditions in combination with other stressors and environmental conditions (i.e., elevated temperature, nutrient levels and daytime versus nighttime) are a critical next step in elucidating coral calcification mechanisms under future ocean conditions.

Methods

Coral collection and preparation. The measurements focused on three species of corals: *O. faveolata, T. reniformis* and *A. millepora*. All species contain photosynthetic endosymbionts, often called zooxanthellae (*Symbiodinium* spp.), and form an aragonite skeleton. Small fragments of *O. faveolata* were sampled from the Florida Keys and transported to the laboratory in the University of Georgia (Florida Keys National Marine Sanctuary permit 2014–2015). *Turbinaria reniformis* and *Acropora millepora* coral fragments were provided by Reef Systems Coral Farm in New Albany, OH. The parent colonies of both species have been maintained in recirculating indoor aquaria with natural light (greenhouse, 700–1000 μmol photons $m^{-2} s^{-1}$) and commercially available artificial seawater (Instant Ocean Reef Crystals) for over 10 years. Several fragments of each colony were shipped to the Cai lab at the University of Georgia, where they were acclimated to a closed-system laboratory aquarium with artificial seawater of salinity 35 and TA of 2.4 mmol kg^{-1} at 26 °C with light levels of about 200 μmol photons $m^{-2} s^{-1}$ for at least two weeks prior to conducting pH and CO_3^{2-} microelectrode profile measurements. TA in the aquarium was depleted at the time of microelectrode measurements (Supplementary Tables 2, 3 and 4) but was amended weekly.

Microelectrode construction and properties. pH microelectrodes[32,33] and CO_3^{2-} microelectrodes[34,35] were constructed as previously described. We made our microelectrodes with a flat tip of diameter between 10 and 15 μm (Supplementary Fig. 3), which enabled us to make pH measurements along a profile into the coral polyp. pH microelectrodes were calibrated with three commercial pH NBS standards (pH = 4, 7 and 10) at 26 °C to determine their response slopes. CO_3^{2-} microelectrodes were calibrated in CO_3^{2-} standard solutions pumped sequentially into a sealed chamber where an electrode was hosted[35]. Carbonate concentrations were set at approximately 50, 150, 250, 350, 500 and 1,000 μmol kg^{-1} by adding controlled amounts of HCl and $NaHCO_3$ into filtered seawater collected from the Gulf of Mexico[35]. Standard solutions were then bubbled with room air for 24 h to minimize further exchange of CO_2 with air during the experiment. Finally, CO_3^{2-} concentrations were precisely calculated by CO2SYS with TA and pH measured by Gran titration and a commercial Ross glass electrode, respectively.

Data collection. In brief, a coral fragment was transferred from the incubation tank together with the tank water into a small measurement chamber that was kept at 26 °C and stirred with a magnetic stirrer (Supplementary Fig. 4). The coral fragment was allowed to acclimate in the small container for 1 h under 500 μmol photons $m^{-2} s^{-1}$ until the microelectrode reading was stable in the chamber water (Fig. 1b & Supplementary Fig. 1). The slopes of pH and CO_3^{2-} microelectrodes were calibrated immediately before use, and chamber water pH measured by a commercial electrode and measured TA values were used as the reference point before beginning the profiles. Measurement conditions are provided in Supplementary Tables 2,3 and 4. The point at which the microelectrode entered the polyp (defined as depth = 0) was observed under a microscope. Typically the coral reacted by closing its mouth making this point unambiguous. The electrode was then advanced through the polyp's gastric cavity in increments of 5–50 μm until the microelectrode broke on the skeleton. The microelectrode was held at each step until a stable reading was obtained. The pH reading was considered stable when drift was <0.2 mV or 0.003 pH min^{-1} (or <0.2 mV min^{-1} for CO_3^{2-}) or a total of 3 min had passed, whichever was first. A 3-min limit was established because our pH microelectrodes had a much shorter response time[32,35] but, in some cases, a stable reading was not realistic due to polyp movement.

Several replicate profiles were obtained to ensure that the microelectrodes were not fouled or otherwise damaged by profiling through the corals. In these tests a profile was obtained about half way through the coral coelenteron, at which point the electrode was returned to the overlying seawater, and the seawater readings were compared with values obtained before profiling was started. Then, the profile was resumed, repeating a portion of the earlier profile to ensure agreement between the two (Fig. 1b and Supplementary Figs 1 and 2). However, this practice cannot be extended into the calcifying fluid as an electrode is destined to be damaged and a repeating profile cannot be collected.

Finally, based on electrode calibration result, stability test and repeated measurements as shown above, we assign errors as ±0.02 pH unit for the overlying seawater, ±0.04 pH unit for the coelenteron and ±0.1 pH unit for the calcifying fluid. For $[CO_3^{2-}]$, a maximum uncertainty of ±10% is established based on our experiences and literature[35,36].

Carbonate chemistry calculation. While the CO2SYS program[37] is popularly used for carbonate equilibrium calculation based on two of the four parameters (TA, DIC, pH and pCO_2), it does not accept the pH and $[CO_3^{2-}]$ pair as input parameters. However, measured pH and $[CO_3^{2-}]$ data allowed us to calculate concentrations of other DIC species, [DIC] and the TA in a straightforward way. For example,

$$[\mathrm{DIC}] = [CO_3^{2-}]([H^+]^2/(K_1{*}K_2) + [H^+]/K_2 + 1) \quad (1)$$

where, K_1 and K_2 are the dissociation constants of the carbonic acid[38]. All equations are described in Supplementary Note 2. As in previous studies, we assumed that the coral's internal salinity was the same as that of the external seawater salinity (that is corals are osmoconformers) for our thermodynamic calculation[5,12,21]. While a lower internal salinity would lead to a higher calculated DIC from the same observed pH and $[CO_3^{2-}]$, for example, calculated [DIC] is 0.8–12% higher at salinity = 30 than that at 35, conclusion derived here holds well within a reasonable salinity range (see more details in Supplementary Note 3). In this work, pH in NBS scale is used. However, when needed, pH in total proton scale is converted to NBS scale roughly by adding 0.15 unit, $pH_{NBS} = pH_T + 0.15$, according to CO2SYS simulation[37] and Dickson[39].

Although internal $[Ca^{2+}]$ was reported to be about 10% higher than that in seawater[23], as it was the only reported value and as seawater $[Ca^{2+}]$ is very high (~10.3 mM), we assumed that $[Ca^{2+}]$ in the calcifying fluid is the same as in seawater in calculating the saturation state Ω. Since $[CO_3^{2-}]$ is directly measured in this work, the uncertainty in Ω calculation is about the same as that in $[Ca^{2+}]$, roughly within 10%, and it does not affect the conclusions and discussion of this work.

Calculation of CO_2 flux into the calcifying fluid. In a 1-D diffusion model, CO_2 molecular diffusional flux is defined as:

$$F_{CO_2} = D_{CO_2}\Delta[CO_2]/\Delta x, \quad (2)$$

where, D is the diffusion coefficient, and Δx is the distance corresponding to the concentration gradient. We assume D determined in seawater[40] is applicable to the coral interior space. We calculated CO_2 flux using the $\Delta[CO_2]$ (Supplementary Table 1) and the corresponding distance between the two data points in the coelenteron and the calcifying fluid, respectively, as observed with our microelectrode (50–100 μm).

Using the calculated $[CO_2]$ gradient (29.8 μmol kg^{-1}) from Supplementary Table 1, CO_2 flux (F_{CO_2}) from the coelenteron into the calcifying fluid was calculated. Note the $[CO_2]$ gradient determined by the microelectrode data is not affected much by the uncertainty caused by relatively large pH and $[CO_3^{2-}]$ ranges inside the calcifying fluid as $[CO_2]$ is nearly 0 (that is an uncertainty of $[CO_2]$ between 0.5 and 0.1 μmol kg^{-1} only changes $[CO_2]$ gradient from 29.9 to 30.3 μmol kg^{-1}) (Supplementary Table 1). In other words, a conservative internal pH value of 9.1 and a high value of 9.5 lead to similar estimates of CO_2 gradient and flux.

Flux can also be calculated as the exchange rate between two adjacent 'boxes', the coelenteron and the calcifying fluid:

$$F_{CO_2} = k_{CO_2}\Delta[CO_2], \quad (3)$$

where, kco_2 is the exchange coefficient (0.76–2.8 cm s^{-1}) across biological tissues determined by an isotopic exchange method[41], which has been used in two recent coral CO_2 flux model simulations[21,26]. In principle, the two coefficients are linked by:

$$k_{CO_2} = D_{CO_2}/\Delta x. \quad (4)$$

A lower CO_2 flux calculated based on equation 3 than equation 2 may indicate that the CO_2 diffusion coefficient across the coral tissue (or the coral tissue's permeability) is lower than that of the seawater.

Amount of H^+-pumping per unit pH upregulation. We define this parameter based on the buffer factor concept, discussed in details by Frankignoulle[42], Hofmann *et al.*[43] and Egleston *et al.*[44]. We take the buffer factor β defined below as a measure of how strong the calcifying fluid can buffer its pH:

$$\beta = \left(\frac{\partial \ln[H^+]}{\partial TA}\right)^{-1} = -\left(\frac{\partial TA}{2.3\partial pH}\right) \quad (5)$$

We rearranged the definition to $\Delta TA/\Delta pH = -2.3\beta$, which represents the amount of proton pumping (or TA gain) a coral must do to upregulate its calcifying fluid pH by one unit. This was calculated numerically by following the same approach as the Revelle Factor calculation in the CO2SYS program[37]. We first set four DIC values and for each DIC value we allowed a range of pH changes. Thus, we derived TA values for the various DIC and pH combinations. Then, a $\pm 1\,\mu mol\,kg^{-1}$ disturbance is applied to TA values and the corresponding perturbation in pH is derived using the TA and DIC pairs as the input parameters in CO2SYS (Fig. 4b).

Energy consumption for pH upregulation. We calculated the relative energy changes of pH upregulation between different OA conditions as specified by Ries[5] using the Nernst equation. The equations and results are given in the Supplementary Note 1 and Supplementary Table 5.

References

1. IPCC. Climate Change 2013. The Physical Science Basis. Contribution of Working Group I to the Fifth Assessment Report of the Intergovernmental Panel on Climate Change (2014).
2. Caldeira, K. & Wickett, M. E. Anthropogenic carbon and ocean pH. *Nature* **425,** 365–365 (2003).
3. Orr, J. C. *et al.* Anthropogenic ocean acidification over the twenty-first century and its impact on calcifying organisms. *Nature* **437,** 681–686 (2005).
4. Hoegh-Guldberg, O. & Bruno, J. F. The impact of climate change on the world's marine ecosystems. *Science* **328,** 1523–1528 (2010).
5. Ries, J. B. A physicochemical framework for interpreting the biological calcification response to CO_2-induced ocean acidification. *Geochim. Cosmochim. Acta* **75,** 4053–4064 (2011).
6. Shamberger, K. E. F. *et al.* Diverse coral communities in naturally acidified waters of a Western Pacific reef. *Geophys. Res. Lett.* **41,** 499–504 (2014).
7. Langdon, C. *et al.* Effect of elevated CO_2 on the community metabolism of an experimental coral reef. *Global Biogeochem. Cycles* **17,** 1011 (2003).
8. Schoepf, V. *et al.* Coral energy reserves and calcification in a high-CO_2 world at two temperatures. *PLoS ONE* **8,** e75049 (2013).
9. Doney, S. C. The growing human footprint on coastal and open-ocean biogeochemistry. *Science* **328,** 1512–1516 (2010).
10. Allemand, D. *et al.* Biomineralisation in reef-building corals: from molecular mechanisms to environmental control. *C. R. Palevol* **3,** 453–467 (2004).
11. Cohen, A. L. & Holcomb, M. Why corals care about ocean acidification: Uncovering the mechanism. *Oceanography* **22,** 118–127 (2009).
12. Allison, N., Cohen, I., Finch, A. A., Erez, J. & Tudhope, A. W. Corals concentrate dissolved inorganic carbon to facilitate calcification. *Nat. Commun.* **5,** 5741 (2014).
13. Venn, A., Tambutté, E., Holcomb, M., Allemand, D. & Tambutté, S. Live tissue imaging shows reef corals elevate pH under their calcifying tissue relative to seawater. *PLoS ONE* **6,** e20013 (2011).
14. Holcomb, M. *et al.* Coral calcifying fluid pH dictates response to ocean acidification. *Sci. Rep* **4,** 5207 (2014).
15. Gagnon, A. C. Coral calcification feels the acid. *Proc. Natl Acad. Sci.* **110,** 1567–1568 (2013).
16. Tambutté, S. *et al.* Coral biomineralization: from the gene to the environment. *J. Exp. Mar. Biol. Ecol.* **408,** 58–78 (2011).
17. Gagnon, A. C., Adkins, J. F. & Erez, J. Seawater transport during coral biomineralization. *Earth Planet. Sci. Lett.* **329–330,** 150–161 (2012).
18. Cohen, A. L. & McConnaughey, T. A. Geochemical perspectives on coral mineralization. *Rev. Mineral. Geochem.* **54,** 151–187 (2003).
19. McConnaughey, T. Zooxanthellae that open calcium channels: implications for reef corals. *Mar. Ecol. Prog. Ser.* **460,** 277–287 (2012).
20. Zoccola, D. *et al.* Bicarbonate transporters in corals point towards a key step in the evolution of cnidarian calcification. *Sci. Rep.* **5,** 9983 (2015).
21. Hohn, S. & Merico, A. Modelling coral polyp calcification in relation to ocean acidification. *Biogeosciences* **9,** 4441–4454 (2012).
22. Kuhl, M., Cohen, Y., Dalsgaard, T., Jergensenl, B. & Revsbech, N. Microenvironment and photosynthesis of zooxanthellae in scleractinian corals studied with microsensors for O_2, pH and light. *Mar. Ecol. Prog. Ser.* **117,** 1995 (1995).
23. Al-Horani, F. A., Al-Moghrabi, S. M. & de Beer, D. The mechanism of calcification and its relation to photosynthesis and respiration in the scleractinian coral Galaxea fascicularis. *Mar. Biol.* **142,** 419–426 (2003).
24. Barott, K. L., Venn, A. A., Perez, S. O., Tambutté, S. & Tresguerres, M. Coral host cells acidify symbiotic algal microenvironment to promote photosynthesis. *Proc. Natl Acad. Sci.* **112,** 607–612 (2015).
25. Agostini, S. *et al.* Biological and chemical characteristics of the coral gastric cavity. *Coral Reefs* **31,** 147–156 (2012).
26. Nakamura, T., Nadaoka, K. & Watanabe, A. A coral polyp model of photosynthesis, respiration and calcification incorporating a transcellular ion transport mechanism. *Coral Reefs* **32,** 779–794 (2013).
27. Barnes, D. J. & Devereux, M. J. Productivity and calcification on a coral reef: A survey using pH and oxygen electrode techniques. *J. Exp. Mar. Biol. Ecol.* **79,** 213–231 (1984).
28. Furla, P., Galgani, I., Durand, I. & Allemand, D. Sources and mechanisms of inorganic carbon transport for coral calcification and photosynthesis. *J. Exp. Biol.* **203,** 3445–3457 (2000).
29. McCulloch, M., Falter, J., Trotter, J. & Montagna, P. Coral resilience to ocean acidification and global warming through pH up-regulation. *Nat. Clim. Change* **2,** 623–627 (2012).
30. Honisch, B. *et al.* Assessing scleractinian corals as recorders for paleo-pH: Empirical calibration and vital effects. *Geochim. Cosmochim. Acta* **68,** 3675–3685 (2004).
31. Jokiel, P. L. Ocean acidification and control of reef coral calcification by boundary layer limitation of proton flux. *Bull. Mar. Sci.* **87,** 639–657 (2011).
32. Zhao, P. & Cai, W.-J. pH polymeric membrane microelectrodes based on neutral carriers and their application in aquatic environments. *Anal. Chim Acta* **395,** 285–291 (1999).
33. Cai, W.-J., Zhao, P. & Wang, Y. pH and pCO_2 microelectrodes measurement and diffusive behavior of carbon dioxide species in coastal marine sediments. *Mar. Chem.* **70,** 133–148 (2000).
34. de Beer, D. *et al.* A microsensor for carbonate ions suitable for microprofiling in freshwater and saline environments. *Limnol. Oceanogr. Meth.* **6,** 532–541 (2008).
35. Han, C., Cai, W.-J., Wang, Y. & Ye, Y. Calibration and evaluation of a carbonate microsensor for studies of the marine inorganic carbon system. *J. Oceanogr.* **70,** 425–433 (2014).
36. Lee, B. H., Shim, Y.-B. & Park, S. B. A lipophilic sol – gel matrix for the development of a carbonate-selective electrode. *Anal. Chem.* **76,** 6150–6155 (2004).
37. Pierrot, D., Lewis, E. & Wallace, D. W. R. *MS Excel Program Developed for CO_2 System Calculations* (Oak Ridge National Laboratory, 2006).
38. Millero, F. J., Graham, T. B., Huang, F., Bustos-Serrano, H. & Pierrot, D. Dissociation constants of carbonic acid in seawater as a function of salinity and temperature. *Mar. Chem.* **100,** 80–94 (2006).
39. Dickson, A. G. pH buffers for sea water media based on the total hydrogen ion concentration scale. *Deep-Sea Res.* **40,** 107–118 (1993).
40. Li, Y. H. & Gregory, S. Diffusion of ions in sea water and in deep-sea sediments. *Geochim. Cosmochim. Acta* **38,** 703 (1974).
41. Sültemeyer, D. & Rinast, K.-A. The CO_2 permeability of the plasma membrane of Chlamydomonas reinhardtii: mass-spectrometric ^{18}O-exchange measurements from $^{13}C^{18}O_2$ in suspensions of carbonic anhydrase-loaded plasma-membrane vesicles. *Planta* **200,** 358–368 (1996).
42. Frankignoulle, M. A complete set of buffer factors for acid-base CO_2 system in seawater. *J. Mar. Syst.* **5,** 111–118 (1994).
43. Hofmann, A., Soetaert, K., Middelburg, J. & Meysman, F. R. AquaEnv: an aquatic acid–base modelling environment in R. *Aquat. Geochem.* **16,** 507–546 (2010).
44. Egleston, E. S., Sabine, C. L. & Morel, F. M. M. Revelle revisited: Buffer factors that quantify the response of ocean chemistry to changes in DIC and alkalinity. *Global Biogeochem. Cycles* **24,** GB1002 (2010).

Acknowledgements

The authors acknowledge financial supports from the NSF EF-1041124 to A.G., 1040940 to M.W., 1041070 to W-J.C., and EF-1315944 to B.H. & W-J.C. D.Q. and X.Y. acknowledge the supports of China Scholarship Council for supporting their visits to the Cai laboratory at the University of Georgia.

Author contributions

W-J.C., A.G., M.W., B.H. and Y.W. conceived and designed the experiments; Y.M., D.Q. and Y.W. performed the experiments; Y.Y., C.H., H.X., B.H. and Y.W. contributed materials/analysis tools; W-J.C. and Y.M. analysed the data, and H.X. and W-J.C. performed the buffer index calculation. W-J.C. prepared the manuscript. All authors contributed to discussion and writing of the paper.

Additional information

Supplementary Information accompanies this paper at http://www.nature.com/naturecommunications

Competing financial interests: The authors declare no competing financial interests.

How to cite this article: Cai, W-J. *et al.* Microelectrode characterization of coral daytime interior pH and carbonate chemistry. *Nat. Commun.* 7:11144 doi: 10.1038/ncomms11144 (2016).

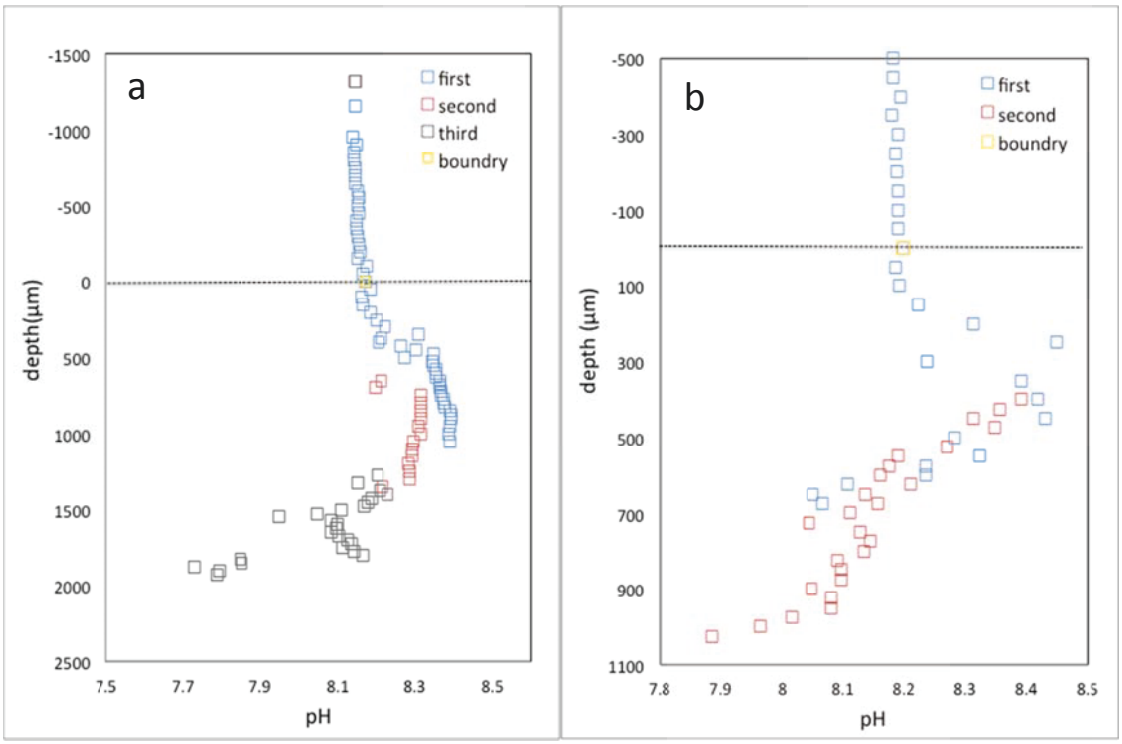

Supplementary Figure 1. pH microelectrode electrode performance and stability test, showing repeated pH_{NBS} microelectrode profile readings inside coral polyps. (a) *T. reniformis* and (b) *A. millepora*. Repeated profiles are listed as first (blue), second (red), and third (gray). The boundary between the coral mouth and seawater is shown with a dashed line bisected by a yellow square.

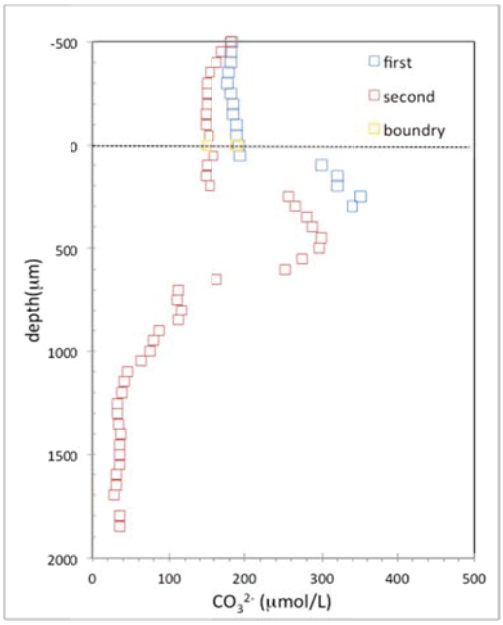

Supplementary Figure 2. Duplicate CO_3^{2-} microelectrode profiles on *T. reniformis.* At the second insert, the polyp contracted, and thus the interface moved down. If the depths are adjusted, the two profiles are highly repeatable. Repeated profiles are listed as first (blue) and second (red). The boundary between the coral mouth and seawater is shown with a dashed line bisected by a yellow square.

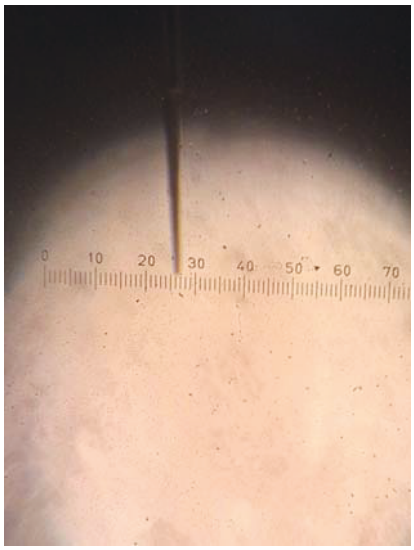

Supplementary Figure 3. pH microelectrode with a tip diameter between 15-20 μm. The microelectrode was photographed at 400x under a dissecting microscope. Note the microelectrode tip is flat and thus the vertical sensing resolution is believe to be only a few μm.

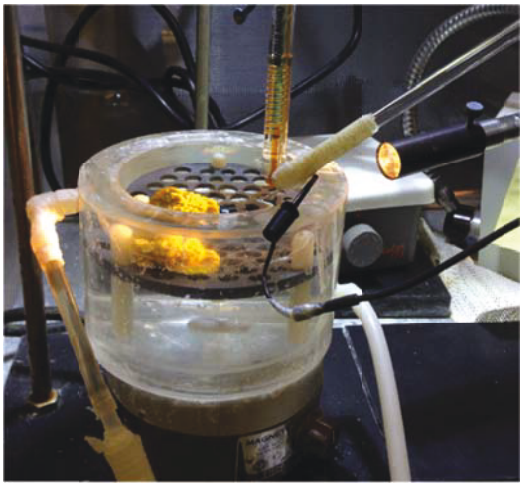

Supplementary Figure 4. Coral microelectrode setup with the coral *Turbinaria reniformis* in the seawater chamber.

Supplementary Table 1. pH, $[CO_3^{2-}]$, DIC, TA, $[CO_2]$ (in μmol kg^{-1}), pCO_2, and Ω_{arag} values inside an average coral polyp

Zone	pH	$[CO_3^{2-}]$	DIC	TA	$[CO_{2aq}]$	pCO_2	Ω_{arag}
Seawater	8.2	183	1479	1759	6.95	252	2.92
Upper coelenteron	8.5	320	1453	1937	3.05	111	5.10
Bottom coelenteron	**7.7**	**80**	**1893**	**1982**	**30.4**	**1100**	**1.28**
Likely combinations of the calcifying fluid	8.7	500	1616	2330	1.90	68.7	7.97
	8.9	700	1685	2649	1.06	38.3	11.2
	9.1	**900**	**1699**	**2907**	**0.54**	**19.6**	**14.3**
	9.5	1100	1489	2962	0.10	3.80	17.5
	10.2	1400	1271	3318	0.01	0.19	22.3
CO_2 flux over 100 or 50 μm distance (mmol $m^{-2}d^{-1}$) Or μmol $cm^{-2}d^{-1}$ Or nmol $cm^{-2}h^{-1}$					51.5-103.0 5.15-10.3 217-433		

Note that data were based on all three species in Fig. 2 across their relative depth profiles plus the highest value from Ref. 1. Upper coelenteron is the first quarter of a profile where a larger pH and CO_3^{2-} increase were observed, usually at 300-500 μm. Bottom coelenteron is the last quarter of a profile, usually 0-500 μm above the calcifying fluid. CO_2 flux calculation into the calcification layer is calculated based on data in the two highlighted rows.

Supplementary Table 2. Measurement conditions for pH_{NBS} and CO_3^{2-} profiles for the coral *Orbicella faveolata*

	Date	Salinity	pH	T (°C)	TA (mmol kg^{-1})
pH1	04/22/2013	35.5	8.26	26.0	1.790
pH 2	05/07/2013	35.0	8.19	26.0	1.701
CO_3^{2-}	08/18/2013	35.0	8.17	26.0	1.700

Supplementary Table 3. Measurement conditions for pH_{NBS} and CO_3^{2-} profiles for the coral *Turbinaria reniformis*

	Date	Salinity	pH	T (°C)	TA (mmol kg^{-1})
pH1	01/09/2015	35.0	8.17	26.0	1.790
pH2	10/07/2012	35.0	8.06	26.0	2.040
CO_3^{2-} 1	07/11/2013	35.5	8.30	26.0	1.690
CO_3^{2-} 2	05/15/2013	35.0	8.24	26.0	2.087

Note that pH2 measurement was carried during nighttime (thus external tank seawater pH was low), but light was on during the microelectrode measurement. All others were collected during daytime.

Supplementary Table 4. Measurement conditions for pH_{NBS} and CO_3^{2-} profiles for the coral *Acropora millepora*

	Date	Salinity	pH	T (°C)	TA (mmol kg^{-1})
pH	09/20/2012	35.0	8.30	26.0	1.790
CO_3^{2-}	08/01/2013	35.0	8.10	26.0	1.611

Supplementary Table 5-part a. Carbonate system constraints and energetic requirements of the calcifying fluid models (low internal DIC)

external pCO_2 (ppm)		TA (umol/kg)	DIC (umol/kg)	pH(NBS)	[H]	HE/HI	ln(HE/HI)	Δ-Energy (%)	Δ-Energy (%)
400	External	2000	1756	8.14	7.213E-09			Ries 2011	Nernst eqn
600	External	2000	1824	7.99	1.014E-08				
900	External	2000	1884	7.84	1.449E-08				
2850	External	2000	2029	7.38	4.214E-08				
400	Internal	2600	1756	8.82	1.5E-09	4.8	1.57063	0.0	0.0
600	Internal	2600	1824	8.75	1.785E-09	5.7	1.73705	18.1	10.6
900	Internal	2600	1884	8.68	2.081E-09	7.0	1.94023	44.7	23.5
2850	Internal	2600	2029	8.52	3.047E-09	13.8	2.62706	187.6	67.3
400	Internal	4000	1756	9.93	1.167E-10	61.8	4.12384	0.0	0.0
600	Internal	4000	1824	9.83	1.465E-10	69.2	4.23711	12.0	2.7
900	Internal	4000	1884	9.75	1.794E-10	80.8	4.39156	30.7	6.5
2850	Internal	4000	2029	9.55	2.848E-10	148.0	4.99716	139.5	21.2
400	Internal	4900	1756	10.42	3.774E-11	191.1	5.25302	0.0	0.0
600	Internal	4900	1824	10.37	4.248E-11	238.7	5.47519	24.9	4.2
900	Internal	4900	1884	10.32	4.763E-11	304.1	5.71749	59.1	8.8
2850	Internal	4900	2029	10.18	6.57E-11	641.4	6.46371	235.6	23.0
400	External	2000	1756	8.14	7.213E-09				
600	External	2000	1824	7.99	1.014E-08				
900	External	2000	1884	7.84	1.449E-08				
2850	External	2000	2029	7.38	4.214E-08				
400	Internal	2804	1756	8.99	1.032E-09	7.0	1.94456	0.0	0.0
600	Internal	2709	1824	8.84	1.452E-09	7.0	1.9432	-0.1	-0.1
900	Internal	2602	1884	8.68	2.073E-09	7.0	1.94424	0.0	0.0
2850	Internal	2348	2029	8.22	6.043E-09	7.0	1.94226	-0.2	-0.1
400	Internal	3825	1756	9.79	1.607E-10	44.9	3.80379	0.0	0.0
600	Internal	3768	1824	9.65	2.259E-10	44.9	3.80405	0.0	0.0
900	Internal	3678	1884	9.49	3.227E-10	44.9	3.8042	0.0	0.0
2850	Internal	3256	2029	9.03	9.393E-10	44.9	3.80371	0.0	0.0
400	Internal	5545	1756	10.62	2.416E-11	298.5	5.69877	0.0	0.0
600	Internal	5163	1824	10.47	3.397E-11	298.5	5.69883	0.0	8.5
900	Internal	4883	1884	10.31	4.847E-11	298.9	5.69996	0.1	8.5
2850	Internal	4400	2029	9.85	1.411E-10	298.6	5.69922	0.0	8.5

Note that part a uses the exact same parameters as in Ries (2011)[1] under relatively low internal DIC conditions. Δ-Energy (%) (Ries 2011) follows the method as in Ries et al. (2011) but Δ-Energy (%) (Nerst eqn) follows the Nerst equation given in Ries et al (2011).

Supplementary Table 5-part b. Carbonate system constraints and energetic requirements of the calcifying fluid models (high internal DIC)

external pCO_2 (ppm)		TA	DIC	pH	[H]	HE/HI	ln(HE/HI)	Δ-Energy (%)	Δ-Energy (%)
400	External							Ries 2011	Nernst eqn
600	External								
900	External								
2850	External								
400	Internal	3900	3200	8.44	3.663E-09	2.0	0.67757	0.0	0.0
600	Internal	3900	3200	8.44	3.663E-09	2.8	1.01816	40.6	50.3
900	Internal	3900	3200	8.44	3.663E-09	4.0	1.3749	100.8	102.9
2850	Internal	3900	3200	8.44	3.663E-09	11.5	2.44277	484.3	260.5
0	Internal	6000	3200	9.53	2.977E-10	24.2	3.18761	0.0	0.0
600	Internal	6000	3200	9.53	2.977E-10	34.1	3.5282	40.6	10.7
900	Internal	6000	3200	9.53	2.977E-10	48.7	3.88493	100.8	21.9
2850	Internal	6000	3200	9.53	2.977E-10	141.6	4.9528	484.3	55.4
400	Internal	7350	3200	10.28	5.304E-11	136.0	4.91263	0.0	0.0
600	Internal	7350	3200	10.28	5.304E-11	191.2	5.25322	40.6	6.9
900	Internal	7350	3200	10.28	5.304E-11	273.1	5.60996	100.8	14.2
2850	Internal	7350	3200	10.28	5.304E-11	794.6	6.67783	484.3	35.9
400	External								
600	External								
900	External								
2850	External								
400	Internal	4206	3200	8.64	2.299E-09	3.1	1.14321	0.0	0.0
600	Internal	4063.5	3200	8.55	2.818E-09	3.6	1.28046	14.7	12.0
900	Internal	3903	3200	8.44	3.644E-09	4.0	1.38007	26.7	20.7
2850	Internal	3600	3200	8.17	6.825E-09	6.2	1.82049	96.9	59.2
400	Internal	5737.5	3200	9.39	4.06E-10	17.8	2.87722	0.0	0.0
600	Internal	5652	3200	9.35	4.474E-10	22.7	3.12085	27.6	8.5
900	Internal	5517	3200	9.28	5.197E-10	27.9	3.32769	56.9	15.7
2850	Internal	4884	3200	8.99	1.027E-09	41.0	3.71417	130.9	29.1
400	Internal	8317.5	3200	10.60	2.519E-11	286.4	5.65731	0.0	0.0
600	Internal	7744.5	3200	10.43	3.71E-11	273.3	5.61054	-4.6	-0.8
900	Internal	7324.5	3200	10.26	5.446E-11	266.0	5.58359	-7.1	-1.3
2850	Internal	6600	3200	9.87	1.349E-10	312.4	5.74417	9.1	1.5

Note that part b is under high internal DIC conditions with TA = 1.5X of the Ries and DIC = 3200 μmol kg^{-1}. Δ-Energy (%) (Ries 2011) follows the method as in Ries et al. (2011) but Δ-Energy (%) (Nerst eqn) follows the Nerst equation given in Ries et al (2011).

Supplementary Note 1

We calculated the relative energy changes of pH upregulation between different OA conditions as specified in Ries [1]. In the literature, Nernst potential across the membrane barrier is defined as (for example, equation 8 of Ries):

$E = (RT)/(nF)\ \ln(H_E/H_I)$,

where H_E and H_I are proton activity (or concentration) in the outside or internal solution respectively. Thus, energy change relative to 400 ppm external pCO_2 should be

$$\Delta E = \{E(pCO_2=x) - E(pCO_2=400)\}\ v/E(pCO_2=400) = \ln(H_E/H_I)_x/\ln(H_E/H_I)_{400} - 1 \qquad (1)$$

According to Table 1 in Reis (2011), he used the ratio of protons directly (i.e., H_E/H_I), not the natural logarithmic form.

In Supplementary Table 4-part a, we calculated both. In either way, energy cost is much smaller for scenario 2 (fixed H_E/H_I ratio) than for scenario 1 (fixed removal). In principle, energy change in scenario 2 should equal to 0 as the ratio H_E/H_I is fixed for all 4 external pCO_2 values. This is exactly reproduced in Supplementary Table 4-part a. Although there appears to be some numerical "noises or errors" in his calculation, the results in Ries Table 1 are generally consistent with the principle.

In Supplementary Table 4-part b, we multiplied the Ries (2011) TA values by 1.5 and set all DIC = 3200 μmol kg^{-1} (roughly a 2X seawater DIC scenario). While we did not try to generate exactly the same H_E/H_I ratios as in Reis, our ranges are quite close. The results show that energy cost of coral responding to ocean acidification due to atmospheric pCO_2 increase would be greater if the coral had a high internal DIC (except the very high pH or very high TA/DIC ratio case when the energy changes are similar for both low and high DIC cases).

Supplementary Note 2

To calculate the carbonate chemistry inside the coral polyp, the measured pH and CO_3^{2-} were used to calculate the other carbonate species using the following equations.

$$[CO_2] = [CO_{2aq}+H_2CO_3] = [H^+]^2*[CO_3^{2-}]/(K_1*K_2) \quad (2)$$

Note in the main text, $[CO_{2aq}+H_2CO_3]$ are simply given as $[CO_2]$. Here, $[CO_{2aq}]$ is the aqueous CO_2 which is >99.5% of the total molecular CO_2 (Ref. [2]). K_1 and K_2 are the first and second dissociation constants of carbonic acid[3].

$$pCO_2 = [CO_{2aq}+H_2CO_3] /K_H \quad (3)$$

$$[DIC] = [CO_2] + [HCO_3^-] + [CO_3^{2-}] = [CO_3^{2-}] ([H^+]^2/(K_1*K_2) + [H^+]/K_2 + 1) \quad (4)$$

$$C\text{-}Alk = [CO_3^{2-}] ([H^+]/K_2 + 2) \quad (5)$$

$$B\text{-}Alk = [B(OH)_4^-] = T_B*K_B/([H^+]+K_B), \quad (6)$$

$$TA = C\text{-}Alk + B\text{-}Alk \quad (7)$$

$$\Omega_{arag} = [Ca^{2+}][CO_3^{2-}]/K_{sp\text{-}arag}, \quad (8)$$

Here, C-Alk and B-Alk are carbon and boron alkalinity respectively. T_B is Total B concentration [4] and K_B is the dissociation constant of boric acid in seawater. $K_{sp\text{-}arag}$ is the solubility constant of aragonite.

Supplementary Note 3

Because salinity inside a coral polyp has not been measured, assuming seawater salinity is the general practice of the community[1,5,6]. Here S = 35 and T = 26°C were used for the calculation. We have also calculated DIC and TA by using a salinity range of ±5. At S=30, DIC is 0.8 to 11.8% higher and TA is 0.4 to 10.8% higher than those at S=35. At S=40, DIC is 0.6 to 8.8% lower and TA is 0.3 to 8.2% lower than those at S=35.

In addition, we performed the calculation using our typical pH(NBS) = 9.5 and $[CO_3^{2-}]$ = 1100 μmol kg^{-1} with several salinities and listed the results in the following table. At salinities 35, 17.5, and 9, we derived [DIC] = 1488.6, 1691.6, and 1951.3 μmol kg^{-1} respectively. Thus for the nature of the conclusions derived here (the range of CO_2 flux and whether internal DIC is 1X of seawater or 2X of seawater) and within a reasonable salinity range, such calculation differences are not important.

Supplementary References

1 Ries, J. B. A physicochemical framework for interpreting the biological calcification response to CO2-induced ocean acidification. *Geochimica et Cosmochimica Acta* **75**, 4053-4064, doi:http://dx.doi.org/10.1016/j.gca.2011.04.025 (2011).

2 Morel, F. M. M. & Hering, J. G. *Principles and Applications of Aquatic Chemistry*. 2nd edn, (John Wiley and Sons, 1992).

3 Millero, F. J., Graham, T. B., Huang, F., Bustos-Serrano, H. & Pierrot, D. Dissociation constants of carbonic acid in seawater as a function of salinity and temperature. *Marine Chemistry* **100**, 80-94 (2006).

4 Lee, K. *et al.* The universal ratio of boron to chlorinity for the North Pacific and North Atlantic oceans. *Geochimica et Cosmochimica Acta* **74**, 1801-1811, doi:http://dx.doi.org/10.1016/j.gca.2009.12.027 (2010).

5 Allison, N., Cohen, I., Finch, A. A., Erez, J. & Tudhope, A. W. Corals concentrate dissolved inorganic carbon to facilitate calcification. *Nat Commun* **5**, doi:10.1038/ncomms6741 (2014).

6 Hohn, S. & Merico, A. Modelling coral polyp calcification in relation to ocean acidification. *Biogeosciences* **9**, 4441-4454, doi:10.5194/bg-9-4441-2012 (2012).